ADVANCED FUNCTIONAL MATERIALS

Supporting Information

for *Adv. Funct. Mater.*, DOI: 10.1002/adfm.201400349

3-Dimensional Tracking of Non-blinking 'Giant' Quantum Dots in Live Cells

Aaron M. Keller, Yagnaseni Ghosh, Matthew S. DeVore, Mary E. Phipps, Michael H. Stewart, Bridget S. Wilson, Diane S. Lidke, Jennifer A. Hollingsworth, and James H. Werner**

WILEY-VCH

Supporting Information

3-Dimensional Tracking of Non-blinking 'Giant' Quantum Dots in Live Cells

Aaron M. Keller, Yagnaseni Ghosh, Matthew S. DeVore, Mary E. Phipps, Michael H. Stewart, Bridget S. Wilson, Diane S. Lidke, Jennifer A. Hollingsworth, James H. Werner**

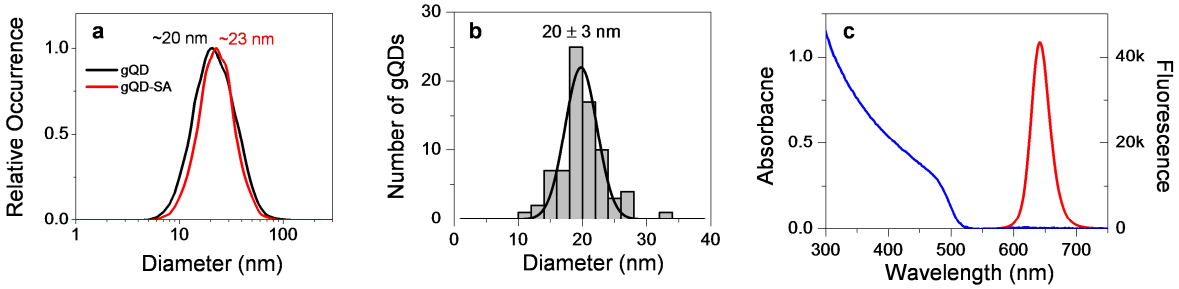

Figure S1. (a) Distribution of hydrodynamic diameters as measured by 2D single-particle tracking for gQD and gQD-SA. gQD has a peak diameter of ~20 nm, while gQD-SA peaks at ~23 nm. The widths of the distributions are not representative of the polydispersity, but are rather attributed to tracking error of the Nanosight instrument. (b) Per particle distribution of gQD diameters as determined by AFM heights. The peak diameter determined through Gaussian fitting is 20 ± 3 nm, which is in agreement with the 2D particle tracking measurement. (c) Absorbance (blue) and fluorescence emission (red) spectra. The emission spectrum peaks at 640 nm. Absorbance and fluorescence data were acquired using a NanoDrop 2000 and 3300 respectively.

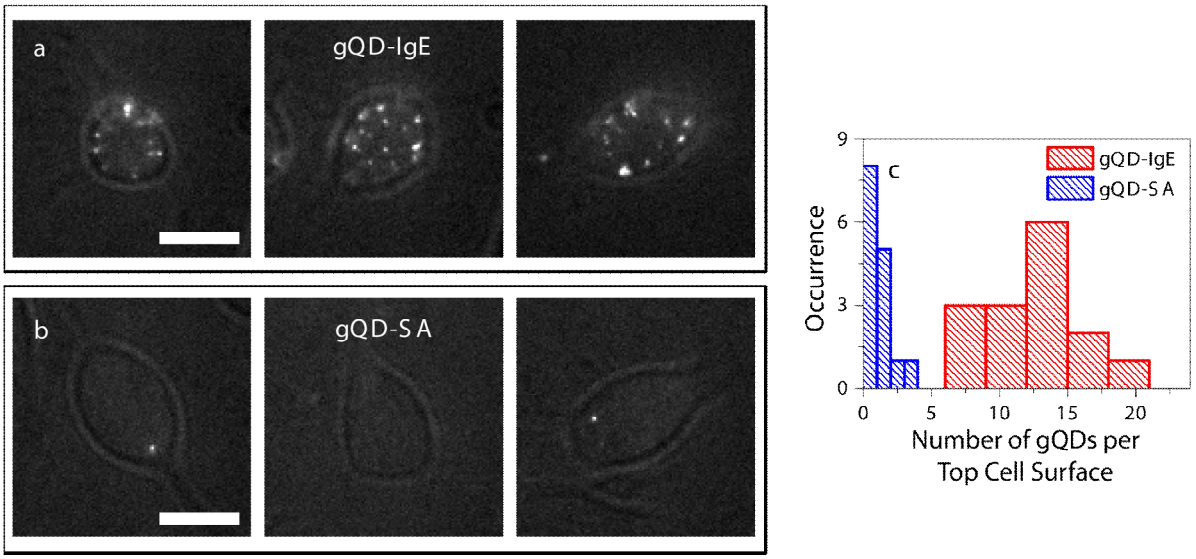

Figure S2. Representative images of RBL-2H3 mast cells incubated with ~1 nM (a) gQD-IgE or (b) gQD-SA. The scale bar is 10 µm. (c) Distribution of the number of gQDs observed on the top of each RBL-2H3 cell for gQD-IgE (red) and gQD-SA (blue).

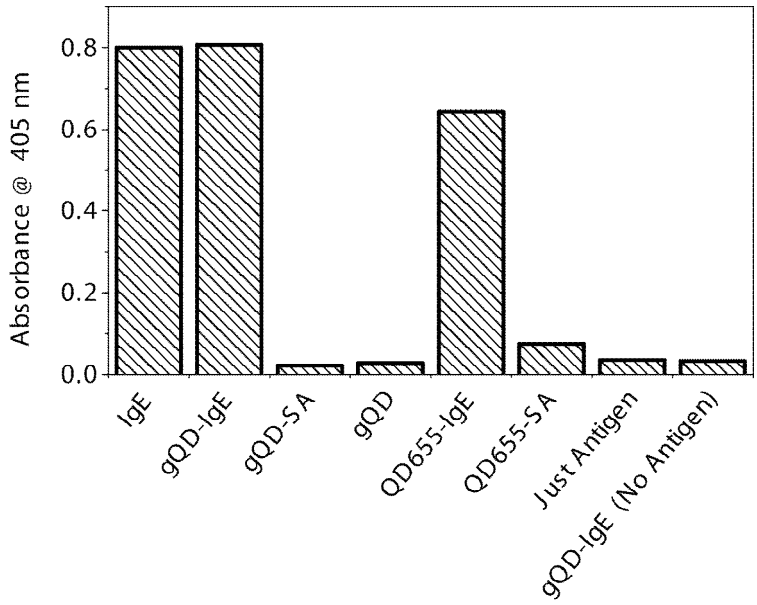

Figure S3. ELISA results showing the absorbance of each well at 405 nm for the oxidized TMB substrate. All wells contained the DNP-BSA antigen with the exception of the last control. The results indicate that only IgE, gQD-IgE, and QD655-IgE show DNP-BSA antigen binding, while all of the controls only showed signal comparable to background.

S1. RBL-2H3 Mast Cell Growth and gQD Labeling

RBL-2H3 cells from the University of New Mexico[1] were cultured in MEM media (Cellgro) supplemented with 10% fetal calf serum, 1% Pen-Strep, and 1% L-Glutamine (Life Technologies), and incubated at 37 °C with 5% CO_2 and 100% humidity. Cells were seeded to chamber slides (Nunc) at densities of 1×10^4 cells per well in 0.5 mL complete MEM without Phenol Red.

After rinsing each well three times with 200 μL of HBSS buffer to remove the MEM media, the cells were incubated for 15 min at 37 °C with 500 pM gQD-IgE in HBSS. After rinsing three times with 200 μL of HBSS, the cells were incubated for 30 min at 37 °C with 1 μg/mL unlabeled IgE to fully activate all the FcεRI receptors. After again rinsing three times with 200 μL of HBSS, the cells were ready for 3D tracking where they remained heated to ~35 °C using an objective heater (TC-1-100, Bioscience Tools). To stimulate the RBL cells, 1–2 μg/mL DNP-BSA in HBSS was added. For tracking of gQD-DNP, the RBL cells were incubated with unlabeled IgE as just described, followed by ~25 pM gQD-DNP in HBSS for ~2 min before rinsing with HBSS.

S2. Determination of gQD Brightness per Particle

The average brightness per particle (BPP) of the gQDs was determined to be ~40 kHz via FCS at the laser power used during our 3D tracking experiments, ~20 μW (**Figure S4**a). The emission of the gQDs filtered with a 640 nm band pass (FF01-641/75, Semrock) was collected by one transmitted and one reflected avalanche photodiode, and cross-correlated by ALV5000 hardware using Equation S1.

$$G(\tau) = \frac{\langle \delta I_A(t) \cdot \delta I_B(t+\tau) \rangle}{\langle \delta I_A(t) \rangle \langle \delta I_B(t) \rangle} \qquad \text{(S1)}$$

Here, $G(\tau)$ is the cross-correlation, $\delta I_X(t)$ represents the deviation in fluorescence intensity of channel X at time t from its average value, and τ represents the lag time. We denote the reflected and transmitted channels by "A" and "B" subscripts. The amplitude of the correlation function, $G(0)$, is equal to $1/N$, where N is the average number of particles in the focal volume. To determine the BPP, the average count rate is multiplied by $G(0)$. FCS could also be used to estimate the concentration of gQDs by dividing N by the approximate excitation volume, ~1 fL. To minimize cross-talk between detectors in the infrared due to after-pulsing, an 800 nm short pass filter was placed in front of each detector (FES0800, ThorLabs).

The distribution of the average gQD-IgE count rate per track is given in Figure S4b. The peak value is ~40 kHz which is consistent with the individual gQD brightness measured by FCS (Figure S4a).

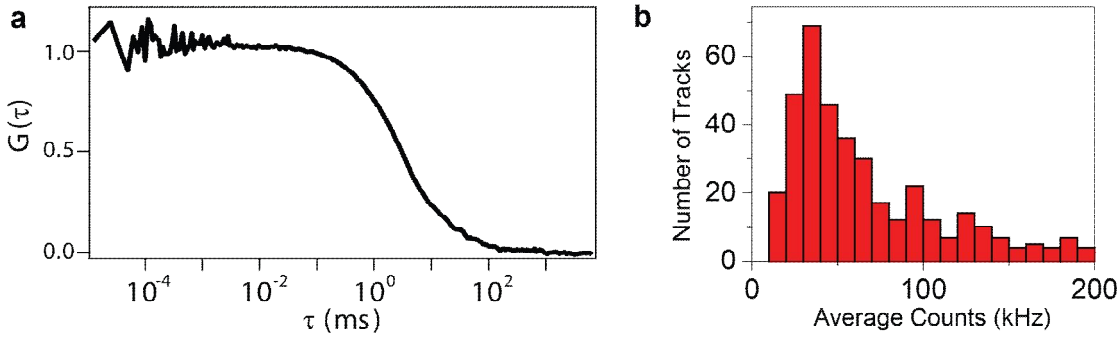

Figure S4. (a) FCS cross-correlation curve of gQDs using 488-nm laser excitation at 20 µW, averaged over four 30 s runs. The BPP of ~40 kHz is determined by multiplying G(0) by the average count rate. The flatness of the curve at shorter τ shows there is no blinking of the gQDs on 0.1 ms to 0.1 µs timescales. (b) Distribution of average count rate per track for 375 gQD-IgE live cell trajectories. The distribution peaks at ~40 kHz which is consistent with the BPP measured by FCS.

S3. Time-Correlated Single Photon Counting

The macro time (given by the number of laser pulses) and micro time (arrival time with respect to each laser pulse) of each photon was recorded using a PicoQuant HydraHarp picosecond event timer. The sample was excited at 405 nm at a repetition rate of 10 MHz with a pulsed diode laser (PicoQuant PDL 800-B). All four channels were synchronized using analog delay boxes (Philips Scientific Dual Delay, Model 792) while measuring a concentrated QD655 reference solution. The instrument response function was measured by looking at the scattering from the coverslip and had a full width at half maximum of ~1 ns. Photon-pair correlation (PPC) histograms were then constructed by computing the absolute photon arrival time (the sum of the macro and micro times) and computing the coincidence of each photon within 4 laser pulses (±400 ns). For time-gating, only photons with micro times between 4 and 20 ns were included in the PPC histogram.

S4. Mean Squared Displacement Analysis

One approach to quantify heterogeneous diffusion is to divide up the trajectory by visual inspection (**Figure S5**a) and then compute the mean squared displacement, $MSD = \langle \Delta x^2 \rangle + \langle \Delta y^2 \rangle + \langle \Delta z^2 \rangle$, as a function of lag time, Δt (Figure S5b) for each region. For Brownian motion, the MSD is linear with a slope of 6*D*, where *D* is the diffusion coefficient. As shown in Figure S5b, *D* spans three orders of magnitude, ranging from ~10^{-3} μm^2/s (essentially immobile) to ~10^{-1} μm^2/s. While this method is valuable for qualitative purposes in assessing the relative rates of Brownian motion, the division of the trajectory into different regions by visual inspection is subjective. In Sections S5 and S6 we explore a more objective approach to quantifying heterogeneous diffusion using a sliding average diffusion coefficient.[25]

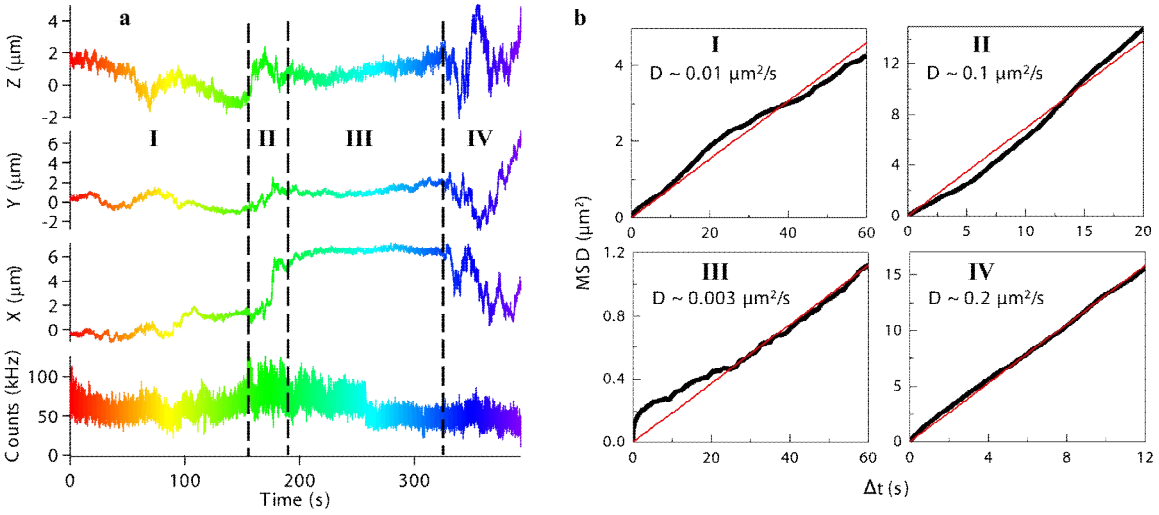

Figure S5. (a) 3D trajectory divided into four different diffusive regimes (I–IV) by visual inspection. (b) Corresponding MSD plots for each region (I–IV). The diffusion coefficient, *D*, for each region varies by three orders of magnitude.

S5. Exploration of Different Time Lags and Averaging Windows for $\hat{D}$

As discussed in the main text, we can compute an average diffusion coefficient, $\hat{D}$, throughout the trajectory using Equation S2.[2]

$$\hat{D} = \frac{1}{6N\Delta t}\sum_{i=1}^{N} MSD_i \qquad \text{(S2)}$$

Ambiguity, however, arises in choosing an appropriate averaging window (N) and lag time, Δt, for which the *MSD* is calculated. To choose appropriate values for each of these parameters, we explore different lag times and window sizes in computing $\hat{D}$ (**Figure S6**) for the trajectory shown previously in Figure S5. To assess which parameter set or sets best represents the heterogeneous diffusion shown in Figure S5, we looked for combinations which could (A) capture the sharp transition in region II, (B) distinguish the subtle motion in region I from the essentially immobile region III, and (C) accurately quantify the fast diffusion in region IV. The shorter lag times, Δt = 50 ms (Figure S6a) and Δt = 100 ms (Figure S6b) fail to capture the sharp

transition in region II while both of the longer lag times, Δt = 250 ms (Figure S6c) and Δt = 500 ms (Figure S6d), are successful at catching this event regardless of window size. The 250-ms lag time does the best at distinguishing between the subtle motion in region I and the immobile region II as shown by the resolution of two slower $\hat{D}$ peaks in Figure S6c. While all lag times and window sizes capture the fast diffusion in region IV, the $\hat{D}$ values contain more noise at smaller window sizes. However, while the larger averaging window sizes contain less noise, the $\hat{D}$ values become systematically smaller because of smoothing with the adjacent diffusion regimes (especially when the dwell time of the diffusion state is comparable to the averaging window). We therefore chose a lag time of 250 ms for our analysis as it satisfies the three aforementioned criteria. We chose an averaging window of 1 s (N = 200) as this value offers a reasonable compromise between noise and smoothing of the $\hat{D}$ values.

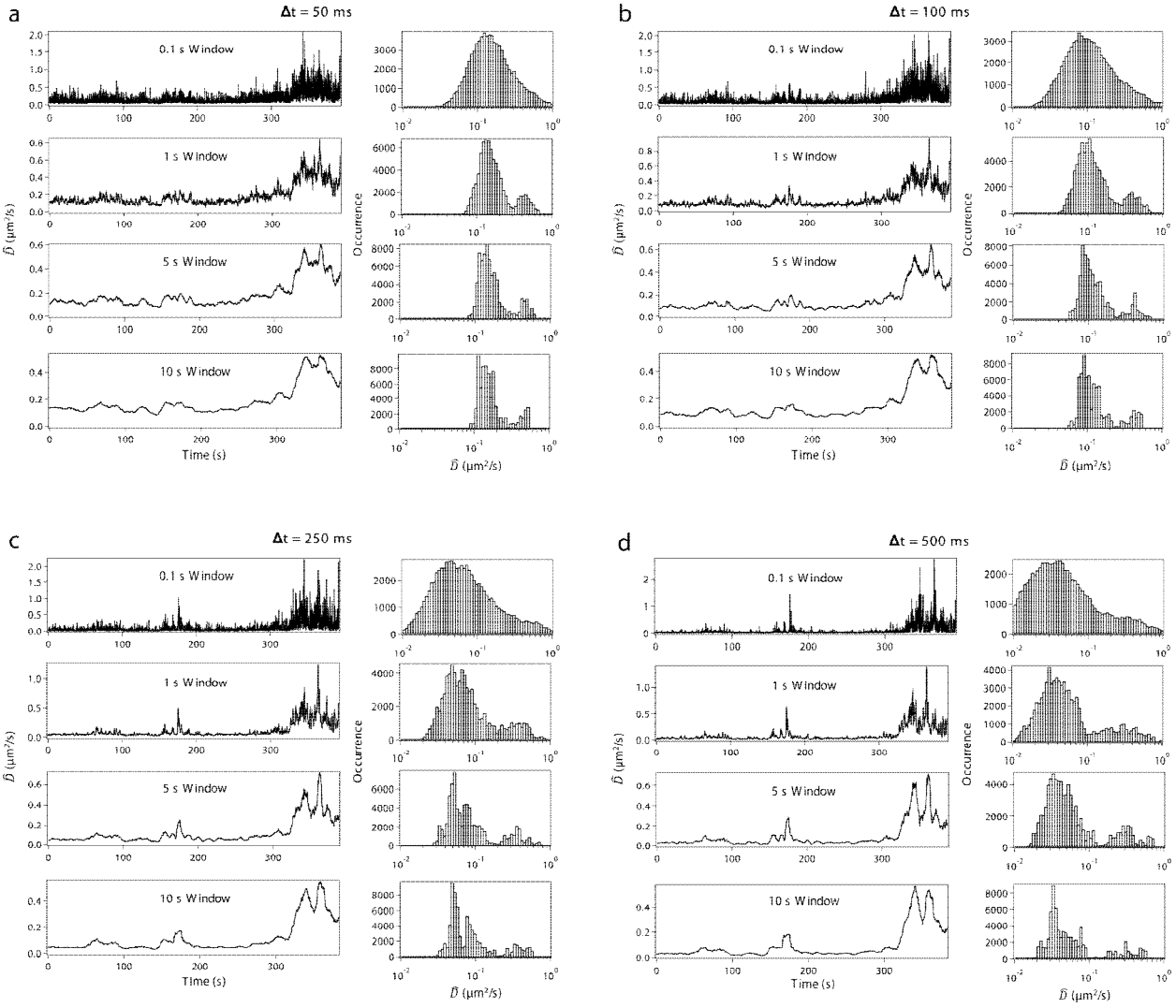

Figure S6. Exploration of different time lags, Δt, and window sizes, while computing the sliding diffusion coefficient, $\hat{D}$ for the trajectory shown in Figure S5. Time lags of (a) 50, (b) 100, (c) 250, and (d) 500 ms are shown along with averaging window sizes of 0.1 s, 1 s, 5 s, and 10 s. The trajectory of $\hat{D}$ vs time along with the histogram of $\hat{D}$ is shown for each parameter set.

S6. vbHMM Analysis

3D trajectories were analyzed with a Variational Bayes Hidden Markov (vbHMM) analysis.[3] Changes in the state of particle's diffusion coefficient were treated as a hidden markov process. The number of diffusion coefficients required to fit the data was determined by imbedding the hidden Markov formalism into a Bayesian analysis. The probability that the data required a specific number of states was calculated by a variational approach to solving Bayes Theorem. The number of states that maximizes this probability is considered to be the appropriate model. Data was fit using the analysis software vbSPT (Variational Bayes for Single Particle Tracking).[3] Default prior parameter values provided with the software were chosen for the analyses with the exception of the initial guess for the range of diffusion coefficient, set as 0.001-10 $\mu m^2/s$.

S7. Additional Example Trajectories Exhibiting Heterogeneous Diffusion

Here we provide examples of additional trajectories showing heterogeneous diffusion (**Figure S7** through **Figure S14**). Supplementary **Movies S2**–**S8** (at 5× real time) and **S9** (at 10× real time) show the 3D evolution of each trajectory through time. The probability of observing such heterogeneity is significantly increased due to the extended tracking duration afforded by the use of non-blinking gQDs. The trajectories shown all have average count rates at or below 100 kHz (including cell background) which is consistent with tracking individual gQDs. We compute $\hat{D}$ for each trajectory as described in Section S5 and in the main text using a Δt of 250 ms and an averaging window of 1 s (N = 200). In addition, we have used vbHMM analysis to quantify the various diffusive states along with their respective dwell times. The following example trajectories all exhibit two to three diffusive states on the order of ~10^{-2}–10^{0} $\mu m^2/s$ with

dwell times ranging from ~10^{-1}–10^{1} s. Although the number of states and dwell times are somewhat dependent upon the initial values used for the priors, the overall conclusion remains unchanged (that multiple states exist with values and dwell times within the ranges we report).

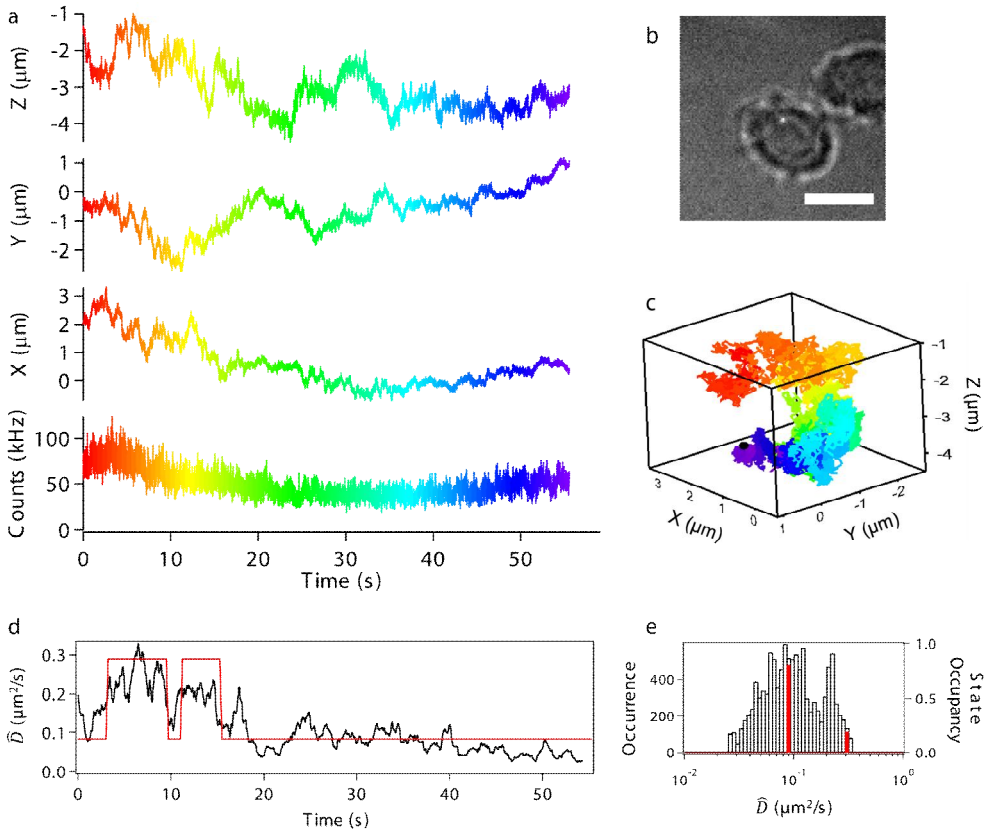

Figure S7. (a) Color-coded total intensity along with x, y, and z position vs. time for unstimulated gQD-IgE. (b) White light image of cell with gQD-IgE in the center (scale bar is 10 μm). (c) 3D trajectory, color-coded with trajectory in (a). (d) $\hat{D}$ vs. time (black) with most probable diffusive state trajectory given by vbHMM analysis (red). (e) Distribution of $\hat{D}$ along with relative occupancy of vbHMM states. For this trajectory, vbHMM analysis suggests two states at ~0.08 and ~0.3 μm^2/s with dwell times of 11 and 3 s respectively.

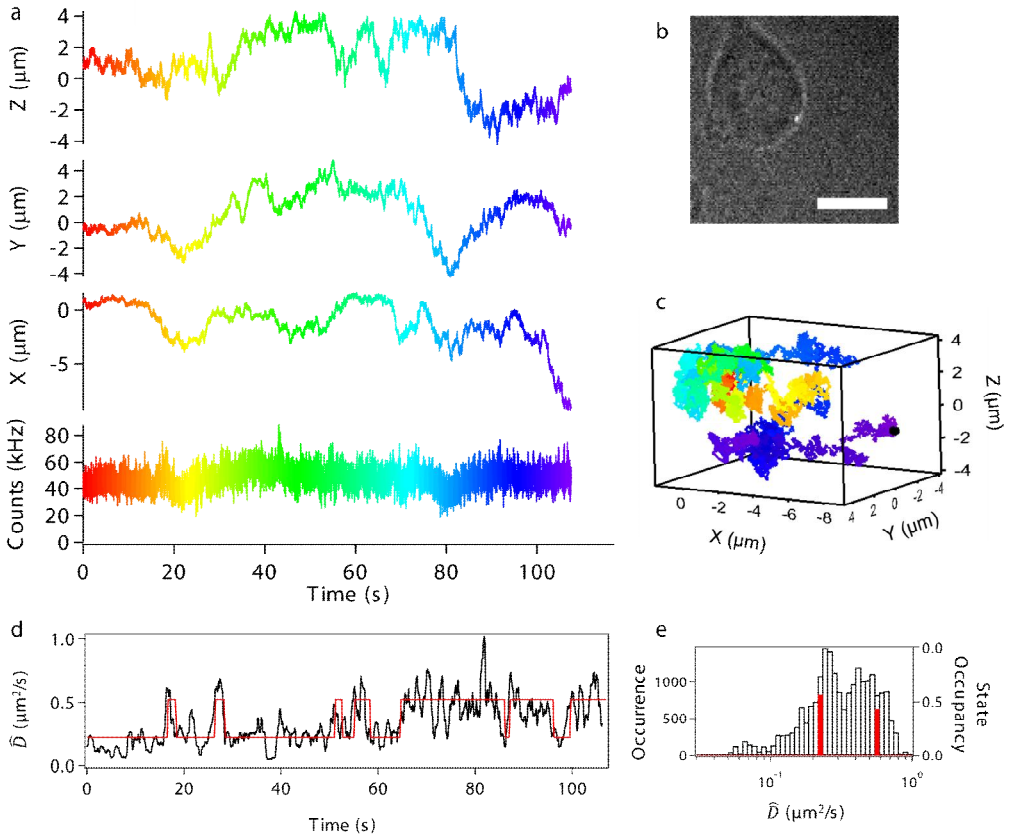

Figure S8. (a) Color-coded total intensity along with x, y, and z position vs. time for gQD-IgE stimulated with 1 µg/mL DNP-BSA. (b) White light image of cell with gQD-IgE in the center (scale bar is 10 µm). (c) 3D trajectory, color-coded with trajectory in (a). (d) $\hat{D}$ vs. time (black) with most probable diffusive state trajectory given by vbHMM analysis (red). (e) Distribution of $\hat{D}$ along with relative occupancy of vbHMM states. For this trajectory, vbHMM analysis suggests two states at ~0.2 and ~0.5 µm^2/s with dwell times of 6 and 5 s respectively.

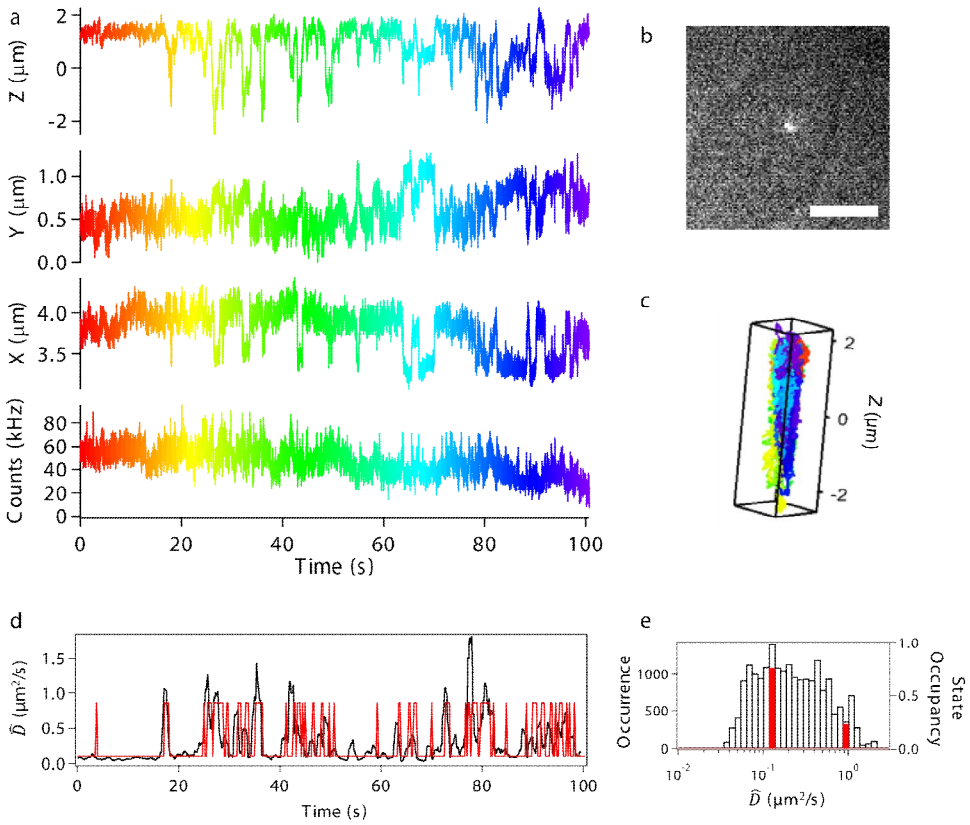

Figure S9. (a) Color-coded total intensity along with x, y, and z position vs. time for gQD-IgE stimulated with 1 µg/mL DNP-BSA. (b) White light image of cell with gQD-IgE in the center (scale bar is 10 µm). (c) 3D trajectory, color-coded with trajectory in (a). (d) $\hat{D}$ vs. time (black) with most probable diffusive state trajectory given by vbHMM analysis (red). (e) Distribution of $\hat{D}$ along with relative occupancy of vbHMM states. For this trajectory, vbHMM analysis suggests two states at ~0.1 and ~0.9 µm^2/s with dwell times of 2 and 0.8 s respectively.

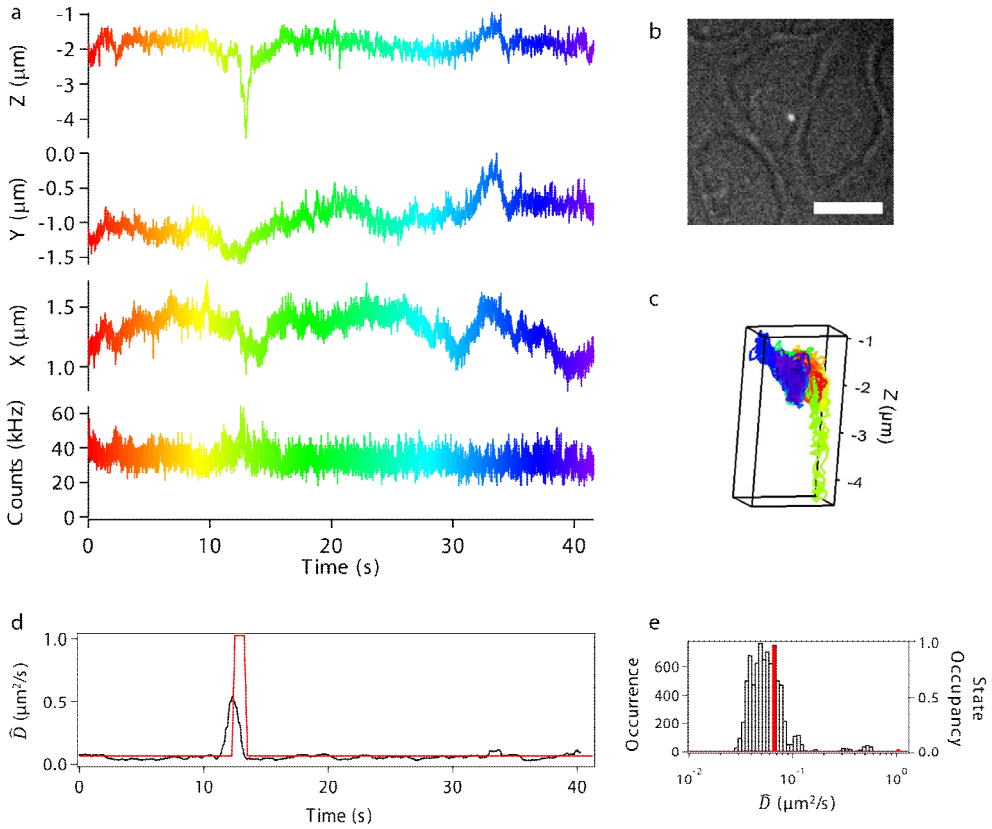

Figure S10. (a) Color-coded total intensity along with x, y, and z position vs. time for unstimulated gQD-IgE. (b) White light image of cell with gQD-IgE in the center (scale bar is 10 µm). (c) 3D trajectory, color-coded with trajectory in (a). (d) $\hat{D}$ vs. time (black) with most probable diffusive state trajectory given by vbHMM analysis (red). (e) Distribution of $\hat{D}$ along with relative occupancy of vbHMM states. For this trajectory, vbHMM analysis suggests two states at ~0.06 and ~1 µm^2/s with dwell times of 14 and 2 s respectively. The $\hat{D}$ value of the higher state is systematically lower than that given by vbHMM analysis because the averaging window size (1 s) is similar to the dwell time of that state (2 s).

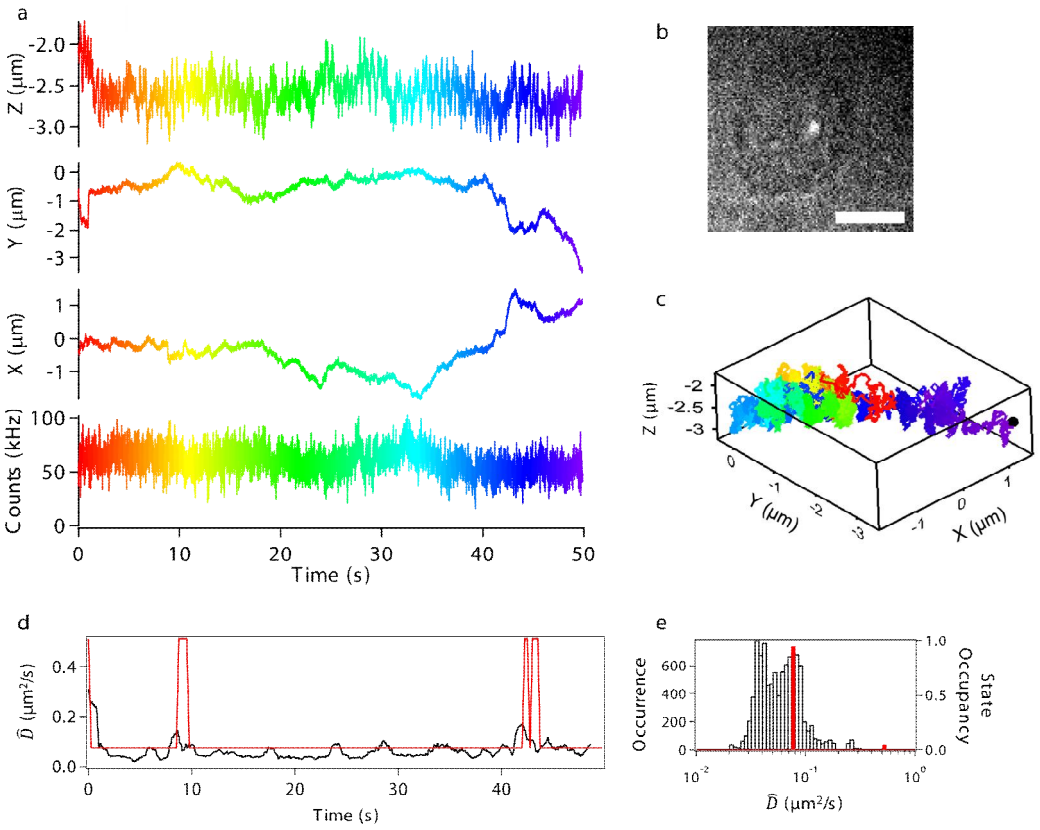

Figure S11. (a) Color-coded total intensity along with x, y, and z position vs. time for gQD-IgE stimulated with 2 µg/mL DNP-BSA. (b) White light image of cell with gQD-IgE in the center (scale bar is 10 µm). (c) 3D trajectory, color-coded with trajectory in (a). (d) $\hat{D}$ vs. time (black) with most probable diffusive state trajectory given by vbHMM analysis (red). (e) Distribution of $\hat{D}$ along with relative occupancy of vbHMM states. For this trajectory, vbHMM analysis suggests two states at ~0.07 and ~0.5 µm^2/s with dwell times of 11 and 1 s respectively. The $\hat{D}$ value of the higher state is systematically lower than that given by vbHMM analysis because the averaging window size (1 s) is similar to the dwell time of that state (1 s).

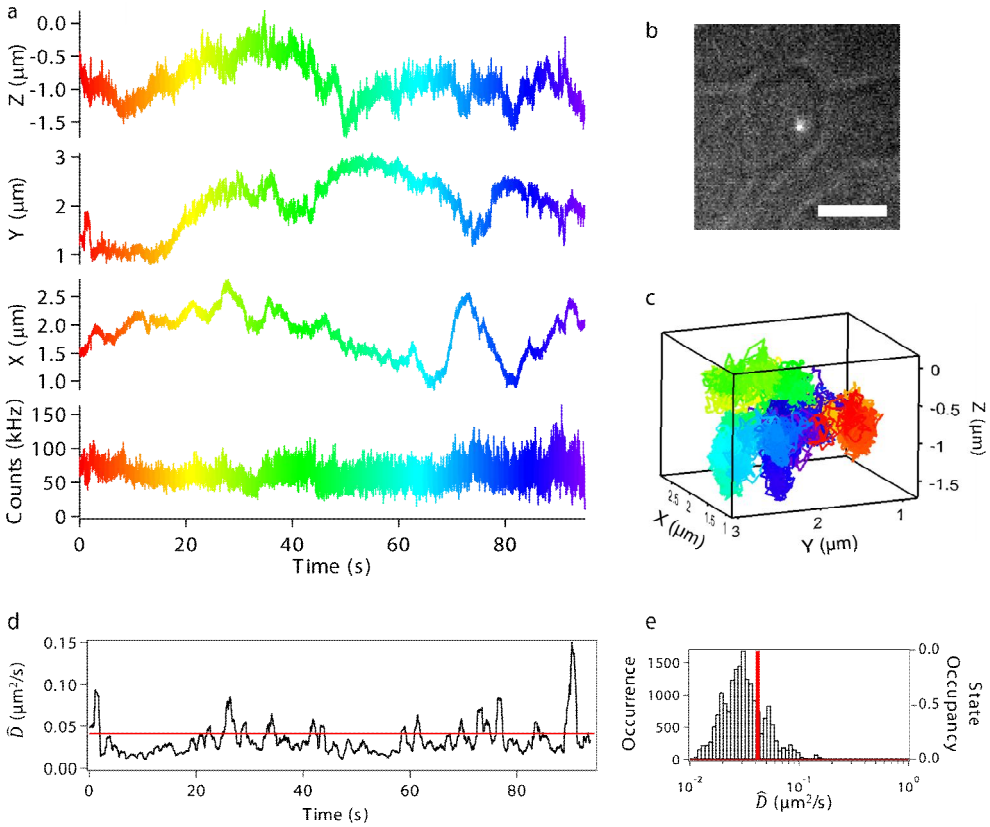

Figure S12. (a) Color-coded total intensity along with x, y, and z position vs. time for gQD-IgE stimulated with 2 µg/mL DNP-BSA. (b) White light image of cell with gQD-IgE in the center (scale bar is 10 µm). (c) 3D trajectory, color-coded with trajectory in (a). (d) $\hat{D}$ vs. time (black) with most probable diffusive state trajectory given by vbHMM analysis (red). (e) Distribution of $\hat{D}$ along with relative occupancy of vbHMM states. For this trajectory, the vbHMM analysis fails to capture multiple diffusive states for the particular set of priors used in the analysis. However, the trajectory and distribution of $\hat{D}$ values clearly show heterogeneous diffusion.

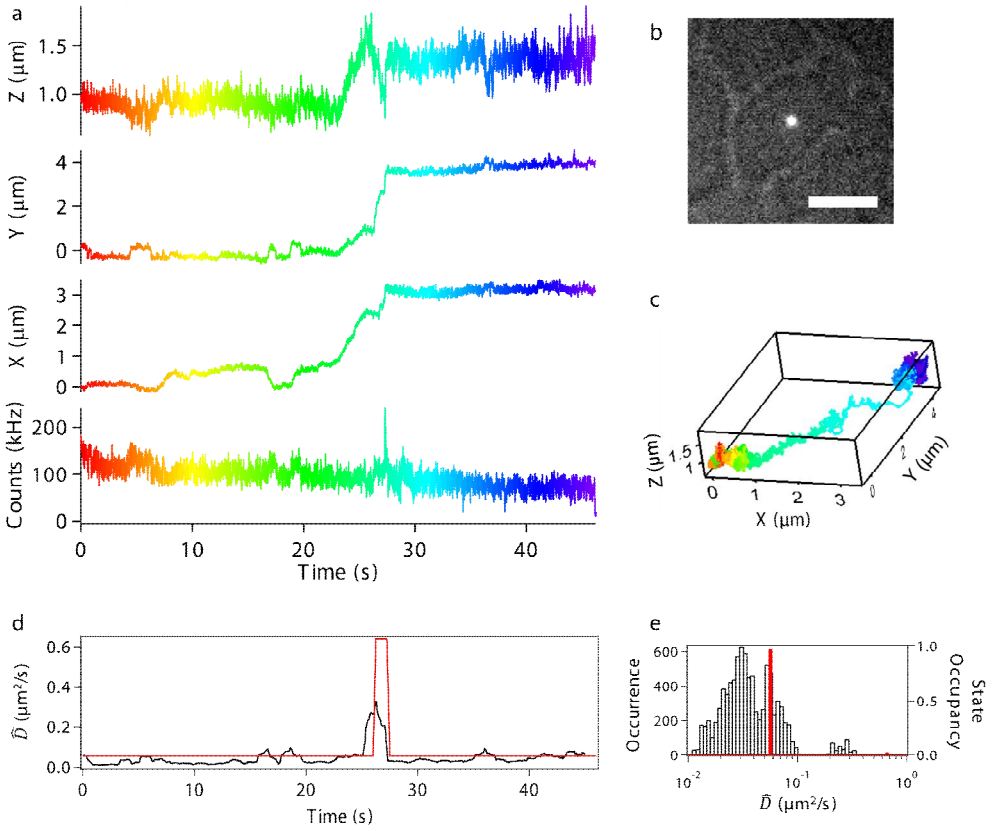

Figure S13. (a) Color-coded total intensity along with x, y, and z position vs. time for gQD-IgE stimulated with 2 µg/mL DNP-BSA. (b) White light image of cell with gQD-IgE in the center (scale bar is 10 µm). (c) 3D trajectory, color-coded with trajectory in (a). (d) $\hat{D}$ vs. time (black) with most probable diffusive state trajectory given by vbHMM analysis (red). (e) Distribution of $\hat{D}$ along with relative occupancy of vbHMM states. For this trajectory, vbHMM analysis suggests two states at ~0.05 and ~0.6 µm^2/s with dwell times of 15 and 2 s respectively. The $\hat{D}$ value of the higher state is systematically lower than that given by vbHMM analysis because the averaging window size (1 s) is similar to the dwell time of that state (2 s).

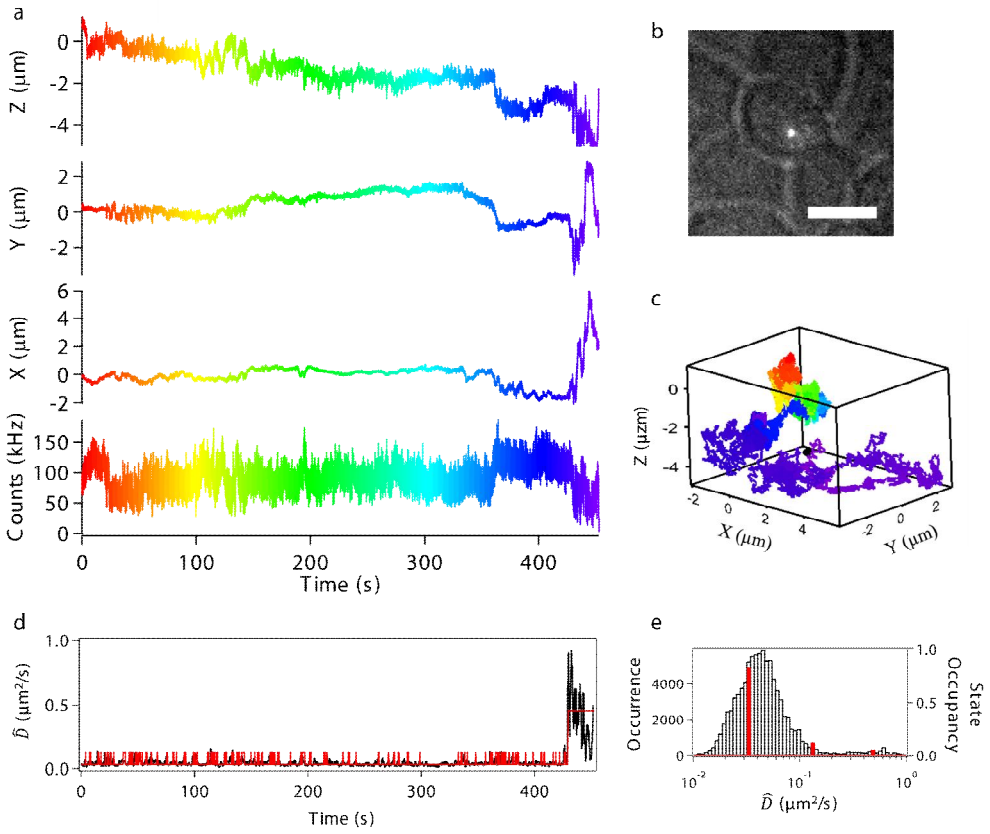

Figure S14. (a) Color-coded total intensity along with x, y, and z position vs. time for gQD-IgE stimulated with 2 μg/mL DNP-BSA. (b) White light image of cell with gQD-IgE in the center (scale bar is 10 μm). (c) 3D trajectory, color-coded with trajectory in (a). (d) $\hat{D}$ vs. time (black) with most probable diffusive state trajectory given by vbHMM analysis (red). (e) Distribution of $\hat{D}$ along with relative occupancy of vbHMM states. For this trajectory, vbHMM analysis suggests three states at ~0.03, ~0.1, and ~0.5 μm^2/s with dwell times of 3, 0.1, and 13 s respectively.

References

[1] N. L. Andrews, K. A. Lidke, J. R. Pfeiffer, A. R. Burns, B. S. Wilson, J. M. Oliver, D. S. Lidke, *Nat. Cell Biol.* **2008**, *10*, 955.

[2] D. Montiel, H. Cang, H. Yang, *J. Phys. Chem. B* **2006**, *110*, 19763.

[3] F. Persson, M. Linden, C. Unoson, J. Elf, *Nat. Methods* **2013**, *10*, 265.